Check for updates

Enhanced thermoelectric performance in n-type polycrystalline SnSe by PbBr$_2$ doping

Debo Li,[ab] Xiaojian Tan,[b] Jingtao Xu,*[b] Guoqiang Liu,[b] Min Jin,[b] Hezhu Shao,[b] HuaJie Huang,[a] Jianfeng Zhang*[a] and Jun Jiang*[b]

A series of PbBr$_2$-doped polycrystalline SnSe samples were synthesized by melting and hot pressing. By PbBr$_2$ doping, the carrier concentration of SnSe was increased to 1.86×10^{19} cm^{-3} from 2.41×10^{17} cm^{-3}, resulting in an increased electrical conductivity of 40 ± 2 S cm^{-1} at 713 K while the undoped SnSe was only 5.1 ± 0.3 S cm^{-1}. Meanwhile, the PbBr$_2$-doped samples also exhibit a larger density of state effective mass ($0.812m_0$). Therefore, a high power factor of 4.8 ± 0.5 µW cm^{-1} K^{-2} and a peak ZT of 0.54 ± 0.1 were achieved at 793 K perpendicular to the hot pressing direction.

I. Introduction

With the progress of society, energy and environmental problems become the most urgent challenges facing mankind in the 21st century. Thermoelectric devices, which enable direct conversion between thermal and electrical energy, have become some of the most promising candidates to meet this challenge.[1–3] The conversion efficiency of a thermoelectric device is determined by the figure of merit ZT of the thermoelectric material. $ZT = S^2\sigma T/\kappa$, where S, σ, κ, and T are the Seebeck coefficient, electrical conductivity, total thermal conductivity (a sum of electronic thermal conductivity κ_e and lattice thermal conductivity κ_l), and the absolute temperature in Kelvin, respectively.[4] To obtain a high ZT, one should enhance the power factor, reduce the thermal conductivity or both simultaneously.

Rock-salt structure IV–VI compounds, such as PbTe, PbSe, and SnTe, are the best thermoelectric materials in the middle to high temperature range (600–920 K).[5–9] Recently, another IV–VI compound SnSe was reported to exhibit a surprising $ZT = 2.6$.[10] The high ZT benefits from the ultralow thermal conductivity (0.23 W m^{-1} K^{-1} at 973 K). SnSe adopts a layered structure crystallized in the orthorhombic *Pnma* space group at room temperature, leading to strong anisotropic properties. The highest ZT of p-type SnSe single crystal is as high as 2.3–2.6 in the *bc* plane and as relatively low as 0.8 along the *a* axis.[10]

The thermoelectric application of SnSe single crystal is seriously limited by the poor mechanical properties and strict growth conditions. Polycrystalline materials are regarded to overcome these difficulties and have been drawing more and more attentions. However, the studies on SnSe polycrystalline were mainly focused on the p-type samples, and the ZTs are much lower than the single crystal.[11–15] In practical applications, p-type and n-type materials are combined to fabricate the p-leg and n-leg of thermoelectric modules, respectively. Thus it is essential to develop the thermoelectric properties of n-type SnSe as well as p-type one.

SnSe is an intrinsic p-type material, and it has been reported that Se loss can induce p–n carrier transition.[16] Halogen doping are found to be an effective way for preparation of n-type SnSe.[17–20] In this work, we chose PbBr$_2$ as the n-type dopant to optimize the carrier concentration and enhance the ZT values of polycrystalline SnSe. Br is an effective dopant to convert SnSe from p-type to n-type semiconductor and Pb can decrease the thermal conductivity for Pb have a heavier relative atomic mass. The anisotropic thermoelectric transport properties of our hot-pressed SnSe polycrystalline are also discussed. Moreover, by comparing with the other halogen doped SnSe, we demonstrate that the increased density of state effective mass also play an important role in the ZT optimization besides carrier concentration turning in our PbBr$_2$ doped SnSe samples.

II. Experimental

The basic materials (Sn granule, 99.999%; Se granule, 99.999%; and PbBr$_2$ powder, 99.99%) were weighed according to the stoichiometric compositions of SnSe$_{0.95}$–x mole% PbBr$_2$ ($x = 0$, 1, 2, 3, and 4) and sealed in high vacuum (10^{-2} Pa) in quartz tubes. The sealed quartz tubes were put into a rocking furnace and heated to 1193 K to melt the materials for 1 h. Then the tubes were taken out of the furnace and air-cooled to room temperature. The obtained ingots were ground into powders in an agate mortar and sieved between 200–300 mesh. The powders were then densified by hot pressing at 753 K for 30 min

^{a}*College of Mechanics and Materials, Hohai University, Nanjing 211100, China. E-mail: jfzhang_sic@163.com*

^{b}*Ningbo Institute of Materials Technology and Engineering, Chinese Academy of Sciences, Ningbo 315201, China. E-mail: xujingtao@nimte.ac.cn; jjun@nimte.ac.cn*

under a pressure of 60 MPa in vacuum to get Ø 12.7 mm × 10 mm pellet.

The phase composition was analyzed by the X-ray diffraction (XRD, Bruker D8) with Cu K_α radiation at room temperature. The fractured and polished surfaces of the samples were observed by the scanning electron microscopy (SEM, Quanta FEG 250). The chemical compositions and the distributions of elements were determined using an energy dispersive X-ray spectrometer (EDXS). The Hall coefficient R_H was measured at room temperature using a physical properties measurement system (Quantum Design PPMS-9) in magnetic fields ranging from −5–5 T. The carrier concentration n and mobility μ were calculated via $n = 1/(eR_H)$ and $\mu = \sigma R_H$, respectively.

The columns were cut into 10 mm × 2 mm × 2 mm bars for electrical property measurement and a disk-shape sample of Ø 8 mm × 2 mm for thermal transport property measurement. The S and the σ were simultaneously measured (ULVAC-RIKO ZEM-3) under a helium atmosphere from 300–793 K. The uncertainty of the Seebeck coefficient and electrical conductivity measurements was 5%. The total thermal conductivity was calculated from $\kappa_{tot} = D\rho C_p$, where D, ρ, and C_p are the thermal diffusivity, the density, and the heat capacity, respectively. The D was measured by the laser flash diffusivity method (Netzsch, LFA-457), ρ was measured using the Archimedes principle and C_p was taken from previous reports.[10] The uncertainty of the thermal conductivity was estimated to be within 8%. The relative density of all the samples is not less than 97% of the theoretical value (6.18 g cm^{-3}). Considering the uncertainties for σ, S and κ, the combined uncertainty for all measurements involved in the calculation of ZT is about 20%.

III. Results and discussions

Strong anisotropic structure is clearly observed in the XRD patterns performed on the samples cut perpendicular and parallel to the pressure directions (Fig. 1a) because of the layered crystal structure of SnSe. The ratio of the integral intensity of plane (400) to plane (111) is 7.96 for perpendicular to the pressing direction and 0.16 parallel to the pressing

direction, respectively. Fig. 1b shows the room temperature XRD patterns for both undoped and doped SnSe polycrystalline samples measured perpendicular to the pressing direction. As seen, the diffraction patterns could be indexed to the orthorhombic phase with a *Pnma* symmetry of SnSe (JCPDS # 48-1224) without any impurity phase.

The degree of orientation of the *bc*-planes is evaluated by the orientation factor $F(400)$, which can be calculated by the Lotgering method according to:[21,22]

$$F = \frac{P - P_0}{1 - P_0} \tag{1}$$

$$P = \frac{I(400)}{\sum I(hkl)} \tag{2}$$

$$P_0 = \frac{I_0(400)}{\sum I_0(hkl)} \tag{3}$$

where P and P_0 are the ratios of the integrated intensities of (400) plane to those of all (hkl) planes for the sintered samples and randomly oriented samples in the angle range 20–60°, respectively. The standard diffraction pattern of SnSe (JCPDS # 48-1224) is used to calculate P_0. The high orientation factor $F(400)$ represents high orientation degree along the (400) plane direction in polycrystalline sample. Based on previous studies in single crystal, high orientation factor $F(400)$ means high σ and κ while small $F(400)$ means low ones. The calculated orientation factor for our samples are summarized in Table 1. It can be seen that the orientation factor $F(400)$ perpendicular to the pressing direction is higher than 0.4 which means a high degree of orientation.

We take SnSe$_{0.95}$–3% PbBr$_2$ as an example to study the microstructure of our samples. As shown in Fig. 2a, the polycrystalline sample (SnSe$_{0.95}$–3% PbBr$_2$ as a representative) exhibits a lamellar microstructure, which is consistent with the layered crystal structure. The lamellar grains with size of 50 μm align along the same direction generally in the fractured surface. Fig. 2b shows the polished surface of the same sample.
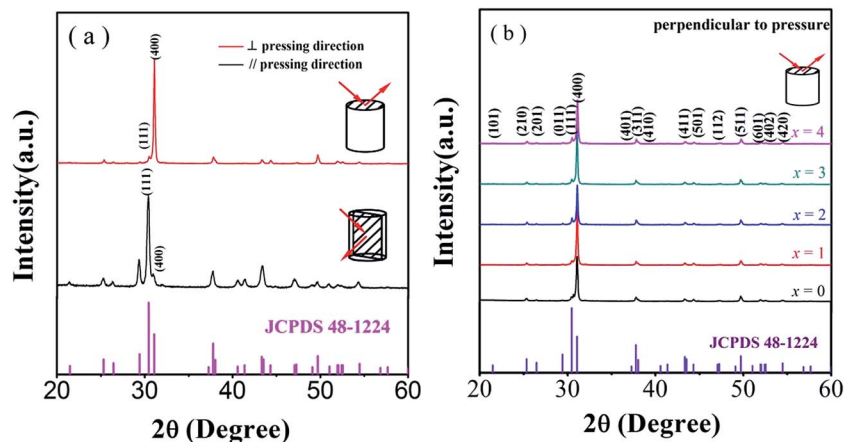

Fig. 1 (a) XRD patterns of the SnSe$_{0.95}$–2% PbBr$_2$ parallel and perpendicular to pressure; (b) XRD patterns of the SnSe$_{0.95}$–x% PbBr$_2$ (x = 0, 1, 2, 3, and 4) perpendicular to pressure.

Table 1 Room temperature carrier concentration, carrier mobility, electrical conductivity, and the orientation factor $F(400)$ plane of $SnSe_{0.95}-x\%$ $PbBr_2$ ($x = 0, 1, 2, 3,$ and 4) samples in the diffraction angle range from $20°$ to $60°$

PbBr$_2$ content (%)	R_H (cm^3 C^{-1})	n (cm^{-3})	σ (S cm^{-1})	μ (cm^2 V^{-1} s^{-1})	$F(400)$
$x = 0$	25.93	2.41×10^{17}	0.46	11.93	0.43
$x = 1$	0.40	1.56×10^{19}	13.33	5.34	0.53
$x = 2$	0.34	1.84×10^{19}	14.88	5.05	0.41
$x = 3$	0.34	1.86×10^{19}	8.80	2.96	0.50
$x = 4$	0.41	1.53×10^{19}	9.71	3.97	0.42

No second phase is observed. The mapping results shown in Fig. 2c–f indicate that the elements of Sn, Se, Br and Pb are all uniformly distributed, suggesting a homogenous doping of PbBr$_2$.

The single crystal of SnSe show strong anisotropic properties due to the layered-like crystal structure. High thermoelectric

Fig. 2 (a) and (b) are the fractured and polished surface morphologies of SnSe$_{0.95}$–3% PbBr$_2$ sample, respectively; (c)–(f) are the EDS mapping for Se, Br and Pb in this sample, respectively.

performance was found along the *bc* plane, while lower thermal conductivity was reported along the *a*-axis. The polycrystalline SnSe samples have also been reported to show anisotropic properties.[10,17,18] But better thermoelectric performance are found in different directions in several reports.[11,17,18] Here, we investigate the anisotropic properties of our PbBr$_2$-doped polycrystalline SnSe samples. The thermoelectric transport properties SnSe$_{0.95}$–2% PbBr$_2$ are measured parallel ($\parallel$) and perpendicular ($\perp$) to the hot pressing direction, and the results are shown in Fig. 3. In Fig. 3a, the electrical conductivity in both directions decreases with increasing temperature to 430 K, and then increases with temperature to 700 K. $\sigma_\perp$ is much higher than $\sigma_\parallel$ in the whole temperature range. The absolute values of the Seebeck coefficient increase with temperature for both directions. The values in the two directions are very close to each other. Therefore, the power factors perpendicular to the hot pressing direction are much larger than the other direction. The highest power factor is 4.33 µW cm^{-1} K^{-2} at 740 K. The thermal conductivity decreases with increasing temperature below 773 K (Fig. 3c). $\kappa_\perp$ is higher than $\kappa_\parallel$ in the whole temperature range, similar to the electrical conductivity. After calculation, higher ZT values are obtained in the direction perpendicular to the pressure, but the anisotropy is much smaller in the ZT values.

Better thermoelectric performance in the direction perpendicular to the pressure is consistent with our previous reports, and other layered-like structure thermoelectric materials, such as Bi$_2$Te$_3$, In$_4$Se$_{3-\delta}$.[23–25] But several groups also reported that higher ZT values in the direction parallel to the pressure.[10,12,14,15,26]

In polycrystalline SnSe samples, the Seebeck coefficients are always reported to be similar in different directions. Therefore, the anisotropy ZT values originate from the ratio of the electrical conductivity to the thermal conductivity. Here, we summarize the ratio of electrical conductivity and the thermal conductivity in two directions from different literatures (Table 2). It can be seen that at 750 K the ratio of $\sigma_\perp/\sigma_\parallel$ to $\kappa_\perp/\kappa_\parallel$ decides higher ZT values in the two direction. We also find that for the reports with higher ZTs in the direction parallel to the pressure, there are two reports which shows larger $\sigma_\perp/\sigma_\parallel$ at room temperature. It seems that the anisotropic degree in electrical conductivity is much more important to determine the overall anisotropic thermoelectric performance.

We now move to the discussion of enhanced electronic transport properties by PbBr$_2$ doping. Fig. 4 summarized the Seebeck coefficient (black dots) at room temperature of
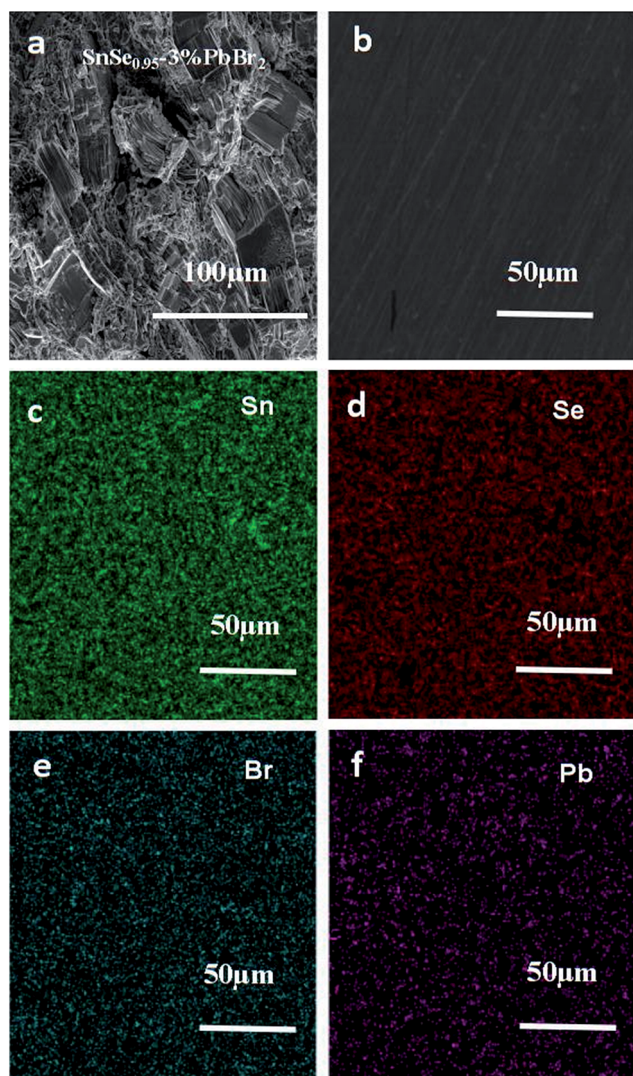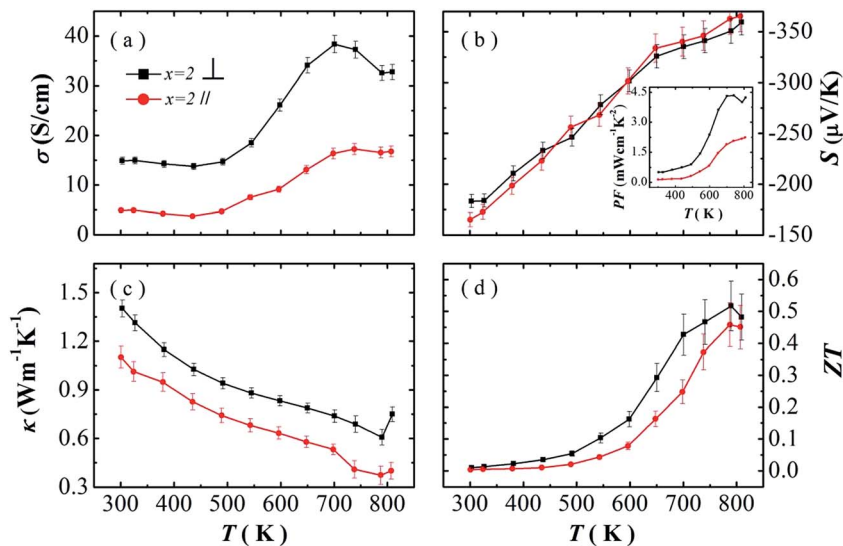
Fig. 3 (a) The electrical conductivity, (b) Seebeck coefficient, (c) thermal conductivity, and (d) ZT as a function of temperature for SnSe$_{0.95}$−2% PbBr$_2$ measured parallel and perpendicular to the pressing direction. The power factor is shown in the inset of (b).

Table 2 Comparisons of the ratio of electrical conductivity and thermal conductivity of perpendicular and parallel to the pressure direction for SnSe samples reported in literatures

	$\sigma_\perp/\sigma_\parallel$		$\kappa_\perp/\kappa_\parallel$		
	300 K	750 K	300 K	750 K	Optimal direction
I-doping Zhang et al.[18]	1.33	0.86	1.60	1.44	$\parallel$
Na-doping Chere et al.[13]	1.80	1.48	1.46	1.23	$\parallel$
Ag-doping Chen et al.[16]	1.24	0.73	1.55	1.58	$\parallel$
SPS SnSe Li et al.[26]	2.51	1.25	1.33	1.45	$\parallel$
S-doping Han et al.[14]	2.35	1.09	1.49	1.42	$\parallel$
Br&Pb-doping Chang et al.[19]	1.96	1.41	1.40	1.40	$\parallel$
BiCl$_3$-doping Wang et al.[17]	2.90	2.15	1.44	1.68	$\perp$
Na-doping Leng, et al.[15]	1.92	2.00	1.42	1.38	$\perp$
Ag-doping Leng, et al.[28]	1.82	1.48	1.33	1.22	$\perp$
PbBr$_2$-doping this work	3.13	2.19	1.27	1.68	$\perp$

SnSe$_{0.95}$−x% PbBr$_2$ ($x = 0, 1, 2, 3,$ and 4) samples as a function of carrier concentration. For comparison, the results of I-doped (blue dots) and BiCl$_3$-doped SnSe (red dots) are also shown.[17,18] It is found that the Seebeck coefficients of these samples are

Fig. 4 Seebeck coefficient as a function of Hall carrier concentration at room temperature for Halogen doped SnSe samples.

similar while the corresponding carrier concentration are very different from one another. To shed light on the undiscovered origin of such difference, we use the single parabolic band model[27] to fit the experimental measurements and plot them in Fig. 4. The Seebeck coefficient and carrier concentration are fitted according to the following equations. (Eqn (4)–(6)) (the scattering factor here is −1/2):
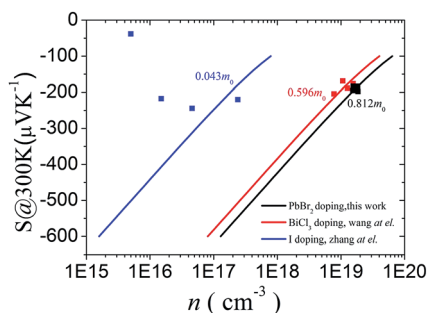
$$S = \frac{k_B}{e}\left[\frac{2F_1(\xi)}{F_0(\xi)} - \xi\right], \tag{4}$$

$$n = \frac{4\pi(2k_B T m^*)^{3/2}}{h^3}F_{1/2}(\xi), \tag{5}$$

$$F_i(\xi) = \int_0^\infty \frac{x^j}{1 + e^{x-\xi}}\,\mathrm{d}x, \tag{6}$$

where ξ and $F_i(\xi)$ are the reduced Fermi energy and the ith order Fermi integral, while h, k_B, e, and m^* are the Plank constant, Boltzmann constant, electron charge, and density of state (DOS)

effective mass, respectively. As shown, the DOS effective mass is $0.043m_0$, $0.596m_0$, and $0.812m_0$ for I-doped, $BiCl_3$-doped, and $PbBr_2$-doped SnSe samples, respectively. As known, a larger DOS effective mass leads to higher Seebeck coefficients at a certain carrier concentration. Due to the small DOS effective mass, the Seebeck coefficient of I-doped SnSe is only 200 μV K^{-1} even with a very low carrier concentration (10^{16} cm^{-3}). Because of the relative large DOS effective mass, the Seebeck coefficient of $PbBr_2$- and $BiCl_3$-doped SnSe show less reduction with increasing the carrier concentration. Comparing our results with the previous $BiCl_3$-doped samples, we find that increasing DOS effective mass is beneficial to enhance Seebeck coefficient of n-type SnSe with electrical conductivity less affected. For example, $SnSe_{0.95}$–4% $PbBr_2$ and $SnSe_{0.95}$–0.1% $BiCl_3$ exhibit similar carrier concentration (1.53 and 1.56×10^{19} cm^{-3}, respectively) and electrical conductivity (9.4 and 9.7 S cm^{-1}, respectively) at 300 K, but the former show significantly higher Seebeck coefficient (−193.3 μV K^{-1}) than the latter (−165.5 μV K^{-1}) because of the larger DOS effective mass. As a consequence, a higher power factor is obtained in $SnSe_{0.95}$–4% $PbBr_2$.

Fig. 5 shows the thermoelectric properties measured perpendicular the hot pressing direction for the $SnSe_{0.95}$–x% $PbBr_2$ (x = 0, 1, 2, 3, and 4) samples: (a) electrical conductivity, (b) Seebeck coefficient, (c) power factor, and (d) thermal conductivity. As Fig. 5a shown, the electrical conductivities could be divided into three stages as reported:[10] first, a metallic transport behavior from 300–500 K; then showing a typical semiconductor behavior up to 750 K; and finally dropping above 750 K. In the temperature range of 300–600 K, the electrical conductivities of x = 1 and 2 is higher than those of x = 3 and 4. This may be attributed to the decrease of mobility caused by enhanced carrier scattering in the samples with larger x. Between 600–800 K, the electrical conductivity shows a significant increase with increasing $PbBr_2$ content and reaches a maximum of 40.2 S cm^{-1} at 713 K for the sample with 3% $PbBr_2$. We summarized the room temperature carrier concentration, mobility and electrical conductivity of the $PbBr_2$-doped SnSe samples in Table 1. As may be seen, the carrier concentration is significantly increased from 10^{17} to 10^{19} cm^{-3} by $PbBr_2$ doping, which indicates $PbBr_2$ is an effective n-type dopant of SnSe. As the $PbBr_2$ content increasing from x = 1 to 3, the carrier concentration increases and mobility decreases, lead to a highest electrical conductivity of 14.9 S cm^{-1} in $SnSe_{0.95}$–2% $PbBr_2$. The decrease in carrier concentration from x = 3 to x = 4 may be caused by the volatilization of $PbBr_2$ (Table 1).

As Fig. 5b shown, the $SnSe_{0.95}$ samples shows the n–p type transition, which is consistent with the results by Chen et al.[16] For the doped systems, the Seebeck coefficients are less dependent on the amount of $PbBr_2$. In the whole measured temperature range, all the $PbBr_2$-doped samples exhibit negative Seebeck coefficients and increased with the increasing temperature. For example, the Seebeck coefficient significantly enhances from −197 μV K^{-1} at 300 K to −363 μV K^{-1} at 793 K for $SnSe_{0.95}$–3% $PbBr_2$.
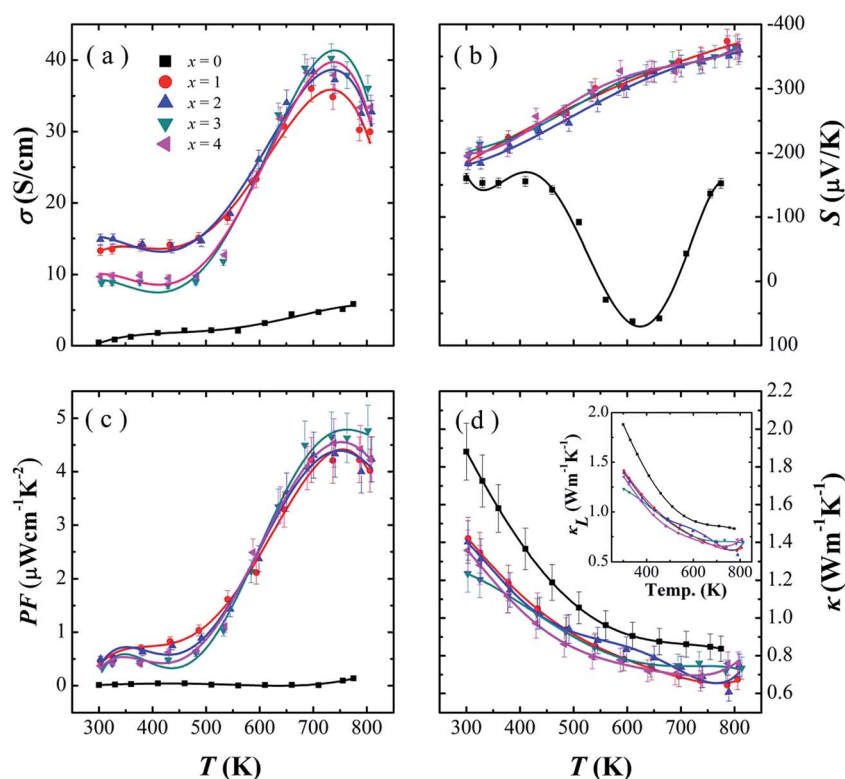

Fig. 5 (a) The electrical conductivity, (b) Seebeck coefficient, (c) power factor, and (d) total thermal conductivity and lattice thermal conductivity for $SnSe_{0.95}$–x% $PbBr_2$ (x = 0, 1, 2, 3, and 4) as a function of temperature.

As may be seen in Fig. 5c, PbBr$_2$-doped SnSe samples exhibit much higher power factors than pristine SnSe$_{0.95}$ due to the significantly increased electrical conductivity. In the whole measured temperature range, the power factor of doped SnSe roughly increases with temperature. The observed highest power factor is 4.8 μW cm^{-1} K^{-2} in SnSe$_{0.95}$–3% PbBr$_2$ at 793 K.

The total thermal conductivity as well as lattice thermal conductivity are shown in Fig. 5d as a function of temperature. The lattice thermal conductivities are calculated by subtracting the electronic contribution from the total thermal conductivities. The electronic contribution is computed using the Wiedemann–Franz law: $\kappa_e = L\sigma T$ where L is the Lorenz number. The Lorenz number L is given as:

$$L = \left(\frac{k_B}{e}\right)\left(\frac{3F_{2(\xi)}}{F_{0(\xi)}}\right) - \left(\frac{2F_{1(\xi)}}{F_{0(\xi)}}\right)^2, \tag{7}$$

where k_B is the Boltzmann constant and the Fermi integral can be obtained from the Seebeck coefficients in Fig. 5b (see eqn (4)).[29] The range of the L values is from 1.5 to 1.7. Due to the poor electrical conductivity, the lattice thermal conductivity is close to the total thermal conductivity. The thermal conductivity are significantly reduced by PbBr$_2$ doping. For example, the room temperature thermal conductivity is 1.88 W m^{-1} K^{-1} in SnSe$_{0.95}$, and it decreases to 1.23 W m^{-1} K^{-1} in SnSe$_{0.95}$–3% PbBr$_2$. In the whole temperature range, the thermal conductivity of all the samples roughly decreases with increasing temperature, and the lowest value is 0.6 W m^{-1} K^{-1} in SnSe$_{0.95}$–2% PbBr$_2$ at 793 K.

Fig. 6 displays the ZT values as a function of temperature for SnSe$_{0.95}$–x% PbBr$_2$ (x = 0, 1, 2, 3, and 4). With increasing temperature, the ZT values are roughly increased until 793 K. For the pristine SnSe$_{0.95}$, the maximum ZT value is ~0.14 at 793 K. By PbBr$_2$ doping, the ZTs are significantly increased and reach a highest value of 0.54 in SnSe$_{0.95}$–3% PbBr$_2$ at 793 K, due to the significantly enhanced electrical transport properties and the reduced thermal conductivity. It should be emphasized that a ZT of 0.54 in PbBr$_2$-doped SnSe samples synthesized by hot pressing is a very conservative value. As the corresponding thermal conductivity (>0.6 W m^{-1} K^{-1} at 793 K) is much higher than the single crystal, there is still room to further increase the ZT of PbBr$_2$-doped SnSe. By nanocomposites or alloys, the thermal conductivity can be decreased and the

thermoelectric performance can be further improved. Recently, a report by Chang *et al.* shows that Pb/Br doped SnSe show a higher ZT of ~1.2 where the thermal conductivity is reduced to 0.3 W m^{-1} K^{-1}.[19]

IV. Summary

The n-type SnSe$_{0.95}$–PbBr$_2$ samples with orientation were synthesized by hot pressing. PbBr$_2$ is proved an effective dopant to significantly increase the carrier concentration, and the samples show negative Seebeck coefficients in the whole temperature range. Our polycrystalline SnSe$_{0.95}$–PbBr$_2$ samples show higher thermoelectric performance in the direction perpendicular to the pressure. As a result of detailed analysis, the DOS effective mass of PbBr$_2$-doped sample is larger than the previously reported n-type SnSe, leading to an enhanced Seebeck coefficient with electrical conductivity less affected. These effects results in a high power factor of 4.8 μW cm^{-1} K^{-2} and a ZT of 0.54 at 793 K in the SnSe$_{0.95}$–3% PbBr$_2$ systems.

Acknowledgements

References

1 L. Bell, *Science*, 2008, **321**, 1457.
2 G. J. Snyder and E. S. Toberer, *Nat. Mater.*, 2008, **7**, 105.
3 A. M. Dehkordi, M. Zebarjadi, J. He and T. M. Tritt, *Mater. Sci. Eng., R*, 2015, **97**, 1.
4 D. M. Rowe, *CRC Handbook of Thermoelectrics: Macro to Nano*, CRC Press, Taylor & Francis, Boca Raton, 2006.
5 K. Biswas, J. Q. He, I. D. Blum, C. I. Wu, T. P. Hogan, D. N. Seidman, V. P. Dravid and M. G. Kanatzidis, *Nature*, 2012, **489**, 414.
6 J. He, X. J. Tan, J. T. Xu, G.-Q. Liu, H. Z. Shao, Y. J. Fu, X. Wang, Z. Liu, J. Q. Xu, H. C. Jiang and J. Jiang, *J. Mater. Chem. A*, 2015, **3**, 19974.
7 G. J. Tan, F. Y. Shi, S. Q. Hao, L.-D. Zhao, H. Chi, X. M. Zhang, C. Uher, C. Wolverton, V. P. Dravid and M. G. Kanatzidis, *Nat. Commun.*, 2016, **7**, 12167.
8 D. Wu, L. D. Zhao, X. Tong, W. Li, L. J. Wu, Q. Tan, Y. L. Pei, L. Huang, J. F. Li, Y. M. Zhu, M. G. Kanatzidis and J. Q. He, *Energy Environ. Sci.*, 2015, **8**, 2056.
9 H. Wang, Y. Z. Pei, A. D. Lalonde and G. J. Snyder, *Adv. Mater.*, 2011, **23**, 1366.
10 L. D. Zhao, S. H. Lo, Y. Zhang, H. Sun, G. Tan, C. Uher, C. Wolverton, V. P. Dravid and M. G. Kanatzidis, *Nature*, 2014, **508**, 373.
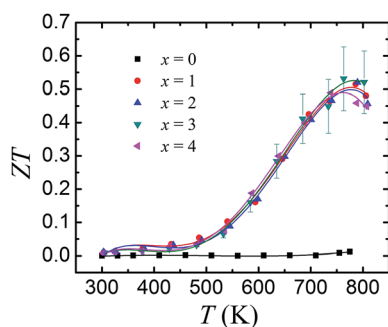

Fig. 6 Temperature dependence of ZT values for SnSe$_{0.95}$–x% PbBr$_2$ (x = 0, 1, 2, 3, and 4).

11 Y. J. Fu, J. T. Xu, G.-Q. Liu, J. K. Yang, X. J. Tan, Z. Liu, H. M. Qin, H. Z. Shao, H. C. Jiang, B. Liang and J. Jiang, *J. Mater. Chem. C*, 2016, **4**, 1201.

12 S. R. Popuri, M. Pollet, R. Decourt, F. D. Morrison, N. S. Bennett and J. W. G. Bos, *J. Mater. Chem. C*, 2016, **4**, 1685.

13 E. K. Chere, Q. Zhang, K. Dahal, F. Cao, J. Mao and Z. F. Ren, *J. Mater. Chem. A*, 2016, **4**, 1848.

14 Y.-M. Han, J. Zhao, M. Zhou, X.-X. Jiang, H.-Q. Leng and L.-F. Li, *J. Mater. Chem. A.*, 2015, **3**, 4555.

15 H.-Q. Leng, M. Zhou, J. Zhao, Y.-M. Han and L.-F. Li, *RSC Adv.*, 2016, **6**, 9112.

16 C.-L. Chen, H. Wang, Y.-Y. Chen, T. Day and G. J. Snyder, *J. Mater. Chem. A*, 2014, **2**, 11171.

17 X. Wang, J. T. Xu, G.-Q. Y. J. Fu, Z. Liu, X. J. Tan, H. Z. Shao, H. C. Jiang, T. Y. Tan and J. Jiang, *Appl. Phys. Lett.*, 2016, **108**, 083902.

18 Q. Zhang, E. K. Chere, K. M. Enaney, M. L. Yao, F. Cao, Y. Z. Ni, S. Chen, C. Opeil, G. Chen and Z. F. Ren, *Adv. Energy Mater.*, 2015, **5**, 1401977.

19 C. Chang, Q. Tan, Y. L. Pei, Y. Xiao, X. Zhang, Y.-X. Chen, L. Zheng, S. K. Gong, J. F. Li, J. Q. He and L. D. Zhao, *RSC Adv.*, 2016, **6**, 98216.

20 A. T. Duong, V. Q. Nguyen, G. Duvjir, V. T. Duong, S. Kwon, J. Y. Song, J. K. Lee, J. E. Lee, S. D. Park, T. Min, J. Lee, J. Kim and S. Cho, *Nat. Commun.*, 2016, **7**, 13713.

21 F. K. Lotgering, *J. Inorg. Nucl. Chem.*, 1959, **9**, 113.

22 L. D. Zhao, B.-P. Zhang, J.-F. Li, H. L. Zhang and W. S. Liu, *Solid State Sci.*, 2008, **10**, 651.

23 Y. B. Zhai, Q. S. Zhang, J. Jiang, T. Zhang, Y. K. Xiao, S. H. Yang and G. J. Xu, *J. Mater. Chem. A*, 2013, **1**, 8844.

24 X. Yan, B. Poudel, Y. Ma, W. S. Liu, G. Joshi, H. Wang, Y. C. Lan, D. Z. Wang, G. Chen and Z. F. Ren, *Nano Lett.*, 2010, **10**, 3373.

25 Y. K. Xiao, G. X. Chen, H. M. Qin, M. L. Wu, Z. P. Xiao, J. Jiang, J. T. Xu, H. C. Jiang and G. J. Xu, *J. Mater. Chem. A*, 2014, **2**, 8512.

26 Y. L. Li, X. Shi, D. D. Ren, J. K. Chen and L. D. Chen, *Energies*, 2015, **8**, 6275.

27 A. F. May, E. S. Toberer, A. Saramat and G. J. Snyder, *Phys. Rev. B: Condens. Matter Mater. Phys.*, 2009, **80**, 125205.

28 H. Q. Leng, M. Zhou, J. Zhao, Y. M. Han and L. F. Li, *J. Electron. Mater.*, 2016, **45**, 1.

29 D. M. Rowe, *CRC Handbook of Thermoelectric*, CRC Press, 1995.